Proceedings of ASME FEDSM'02
2002 ASME Fluids Engineering Division Summer Meeting
Montreal, Quebec, Canada, July 14–18, 2002

FEDSM2002-31434

RECONSTRUCTION OF SOLID AIR TWO PHASE FLOW CT IMAGE USING SAMPLED PATTERN MATCHING METHOD

Masahiro TAKEI
Nihon University, Tokyo Japan
takei@mech.cst.nihon-u.ac.jp

Hui LI
Kagoshima University, Kagoshima Japan

Mitsuaki OCHI
Nihon University, Tokyo Japan

Yoshifuru SAITO
Hosei University, Tokyo Japan

Kiyoshi HORII
Shirayuri College, Tokyo Japan

ABSTRACT

A new reconstruction method, which is called sampled pattern mating method (SPM), has been applied to an ill-posed inverse problem of a capacitance-computed tomography for solid air two-phase flow. As a result, the accuracy of the reconstructed image is improved as compared with a conventional Newton-Rampson iterative method. Moreover, the particles volume ratio in solid air two-phase flow calculated by SPM method is more accurate than the conventional method.

KEYWORD Computed tomography, Solid-air two-phase flow, Image reconstruction, SPM method, Ill posed inverse problem

INTRODUCTION

Recently, a non-invasive real time monitoring technique using computed tomography (CT) gets popular in multiphase flow measurement. In solid-air two-phase flow, capacitance CT with real time visualization has been studied as a technique to visualize solid behavior (Huang,S.M. et al. 1989; Dyakowski,T. et al. 1999). This capacitance CT attaches a sensor consisting of many electrodes around a circumference of a pipeline to measure the capacitances between the electrodes. The particle density distribution based on the permittivity distribution in a cross section is obtained from the experimental capacitances by an image reconstruction technique based on a mathematical ill-posed inverse problem. With regard to the ill-posed inverse problem, roughly, three types mathematical solution technique exist, which are a method with a restraint condition such as linear back projection (LBP) method and least norm method, iterative method such as Newton-Rampson (NR) method, and interpolation or extrapolation method. Moreover, a reconstruction techniques based on artificial neural networks have been developed (Duggan P.M, et al. 1995). A suitable mathematical method for this capacitance CT has been needed because an inverse problem depends on the system equation. In the image reconstruction methods, the method with restraint condition such as LBP method, and iterative method such as NR method are widely used. For example, LBP is the first algorithm; however, the images obtained by LBP are so blurred because the approximate values are not compensated with the physical background of the reconstructed image (Xie,C.G, et al. 1992). NR method is much popular; however, it needs gain setting to converge the image error during the iteration, which is not satisfactory to reconstruct an image accurately because NR does not have the evaluation function and does not confirm if the solution is stable or not at the iterative process (Liu,S. et al. 2001). To overcome the demerit of NR method, Model-based reconstruction (MOR) algorithm and Algebraic reconstruction technique (ART) are developed. MOR algorithm is a method to minimize the discrepancy between the measured and estimated capacitances by altering the dielectric constant distribution described by parameters (Isaksen O et al.1993). ART is a method to improve the initial images using the LBP by iterative scheme by altering the medium distribution as function of the difference between the measured and calculated normalized capacitances and the sensitivity information (Reinecke N and Mewes D 1994).

The originality of this paper lies in launching a new reconstruction method, which is called sampled pattern matching method to apply to the reconstruction of the particles distribution images. As a preliminary study, a simulation is carried out to examine the characteristics of SPM method, and applying it to the real particle image to calculate the relative void ratio in order to discuss the availability of SPM.

PRINCIPLE OF CAPACITANCE TOMOGRAPHY

The capacitance CT sensor is shown in Figs.1 (A) and (B). Insulation materials separate the 12 electrodes in the sensor. The relation between capacitance and permittivity in the static electro field is expressed by:

$$C_{i,j} = -\frac{\varepsilon_0}{V_c} \oint_{r \subseteq \Gamma_j} \varepsilon(\mathbf{r}) \nabla V_i(\mathbf{r}) \cdot d\mathbf{r} \qquad (1)$$

Where, i is the standard electrode number which is from 1 to 11, and j is the reference electrode number which is from i+1 to 12. $C_{i,j}$ is the capacitance between the standard electrode i and the reference electrode j. ε_0 is the vacuum permittivity of air, $\varepsilon(\mathbf{r})$ is the permittivity distribution on the cross section. $\mathbf{r}$ is a position vector on the cross section. V_c is a voltage to the i electrode. Γ_j is an area affected by the electric line of force. $V_i(\mathbf{r})$ is the potential distribution on the cross section between i and j electrodes. Because $V_i(\mathbf{r})$ is unknown in Eq.(1), Laplace equation:

$$\nabla \cdot [\varepsilon(\mathbf{r}) \nabla V(\mathbf{r})] = 0 \qquad (2)$$

is assumed in the cross section. $V(\mathbf{r})$ is obtained from the discretized Eq.(2). The matrix expression in Eq.(1) showing the relation between the capacitance matrix **C** and the permittivity distributions **E** is :

$$\mathbf{C} = \mathbf{S_e E} \qquad (3)$$

Where, the sensitivity map matrix $\mathbf{S_e}$ consists of the known values of ε_0, V_c and $\nabla V_i(\mathbf{r})$ in Eq.(1). In other words, the capacitance CT has a method to obtain the permittivity distribution of the particles **E** in the cross section from both known sensitivity map matrix $\mathbf{S_e}$ and measured capacitance matrix **C**. In the case of 12 electrodes and 32×32 = 1024 pixel as the space resolution as shown in Fig.(c) in the pipeline cross section, the sensitivity map $\mathbf{S_e}$ is a 66×1024 matrix in Eq.(3), the capacitance matrix **C** expresses a 66×1 matrix, and the permittivity distribution matrix **E** is a 1024×1 matrix. The mathematical method to obtain the permittivity matrix **E** from both the capacitance matrix **C** and the sensitivity map matrix $\mathbf{S_e}$ is ill-posed inverse problem because the inverse matrix $\mathbf{S_e}^{-1}$ does not exist. Fig.2 shows the two-dimensional distribution revised 1st row to 6th row of the sensitivity map matrix $\mathbf{S_e}$. They mean kinds of particle potential distributions in the two-dimensional cross section.

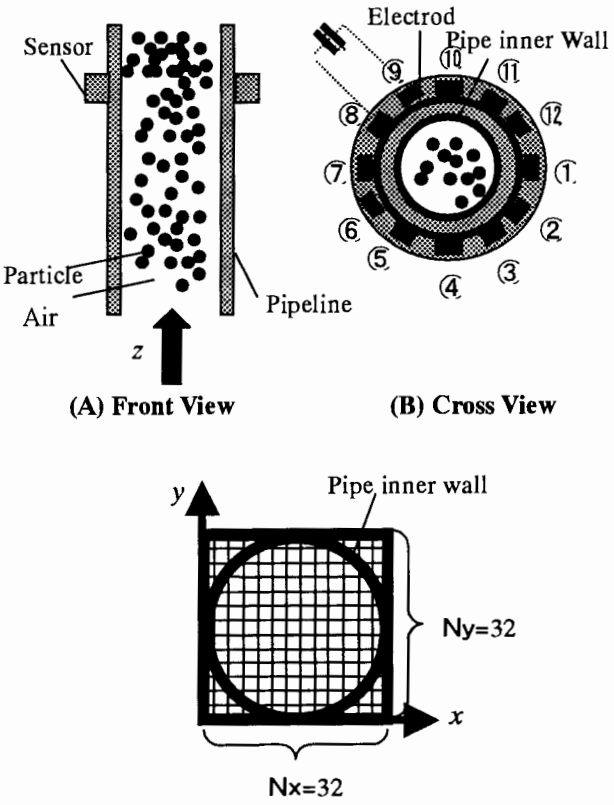

(A) Front View **(B) Cross View**

(C) Space Resolution

Fig. 1 Overview of Capacitance Tomography and Its Space Resolution

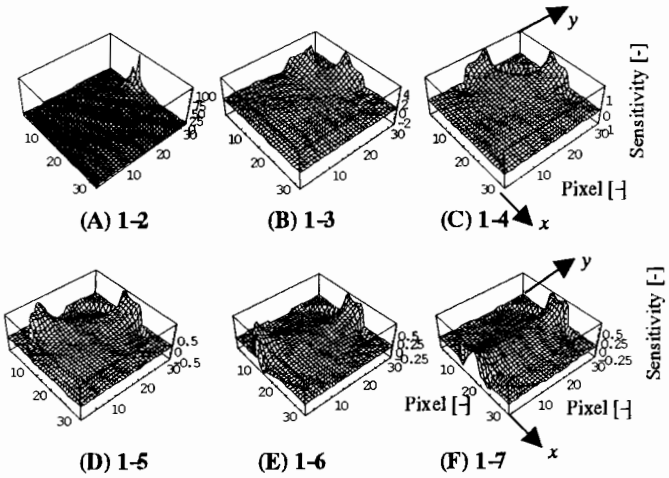

(A) 1-2 **(B) 1-3** **(C) 1-4**

(D) 1-5 **(E) 1-6** **(F) 1-7**

Fig.2 Sensitivity map matrices
(Standard electrode 1 –Reference electrode from 2 to 7)

THEORY OF SPM METHOD

Characteristics of SPM

Basically, the sampled patterned matching method is an iterative method; however, the method has two characteristics that another different method does not have, which are normalization of the system equation by norm, and an evaluation function. As a result, SPM method converges a reconstructed permittivity image stably during the iteration without setting a gain value. From Eq.(3), the capacitance matrix $\mathbf{C}$ can be expressed by ith column vector of $\mathbf{S_e}$: $\mathbf{S_{ei}}$, and ith element of $\mathbf{E}$: e_i, that is:

$$\mathbf{C} = \mathbf{S_e}\mathbf{E} = \sum_{i=1}^{m} (\mathbf{S_{ei}} e_i) \tag{4}$$

Where, m is the space resolution: m=1024. Eq.(4) normalized by the norm is:

$$\frac{\mathbf{C}}{|\mathbf{C}|} = \sum_{i=1}^{m} \left(\frac{\mathbf{S_{ei}}}{|\mathbf{S_{ei}}|} \frac{e_i}{|\mathbf{C}|/|\mathbf{S_{ei}}|} \right)$$

$$\mathbf{C}' = \sum_{i=1}^{m} (\mathbf{S_{ei}}' e_i') = \mathbf{S_e}'\mathbf{E}' \tag{5}$$

Where, the prime is the normalization by the norm, $|\ |$ is the norm. For instance, the norm of $\mathbf{C}$ is square root of square sum of each element:

$$|\mathbf{C}| = \sqrt{c_1^2 + c_2^2 + \bullet\bullet\bullet + c_n^2} \tag{6}$$

Where, n is the total pair number of the electrodes: n=66.

The other characteristic is an evaluation function to indicate if a solution is converged using an inner product between the capacitance of kth iterative permittivity: $\mathbf{C}^{(k)}$ and the experimental capacitance: $\mathbf{C}^{(0)}$. The evaluation function of $\mathbf{E}^{(k)}$: $\mathbf{f}(\mathbf{E}^{(k)})$, is set up by:

$$\mathbf{f}(\mathbf{E}^{(k)}) = \mathbf{C}'^{(0)}\,\mathbf{C}'^{(k)} \rightarrow 1.0 \tag{7}$$

The permittivity distribution by SPM method is $\mathbf{E}^{(k)}$ when $\mathbf{f}(\mathbf{E}^{(k)})$ becomes near 1.0. To simplify the explanation, in the case of three capacitance elements: n=3 (the vector can be drawn in Cartesian coordinates), the converging process by SPM can be expressed by Fig.3. In the iterative process, the sampled vector $\mathbf{C}^{(k)}$ becomes the experimental vector which is the experimental capacitance: $\mathbf{C}^{(0)}$ because the inner product becomes nearly 1.0.

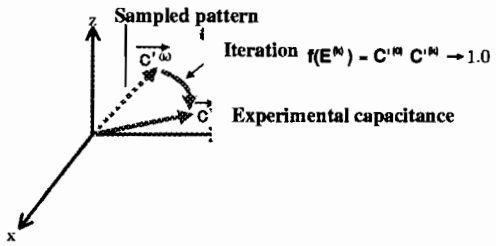

Fig.3 Outline of SPM

Iterative Solution by SPM Method

SPM method dose not limit an iterative method. In this study, an iterative solution from LBP initial permittivity image is used. When the initial capacitance obtained from the experiment is $\mathbf{C}^{(0)}$ and the initial value of $\mathbf{E}$ by LBP is $\mathbf{E}^{(0)}$, from Eq.(5), the normalized $\mathbf{E}^{(0)}$ is:

$$\mathbf{E}'^{(0)} = \mathbf{S_e}'^{\mathrm{T}}\,\mathbf{C}'^{(0)} \tag{8}$$

Where, $\mathbf{Se}^{\mathrm{T}}$ is the transpose matrix of $\mathbf{S_e}$, $\mathbf{E}^{(0)}$ is an approximate value because $\mathbf{Se}^{\mathrm{T}}\mathbf{S_e}$ dose not become an unit matrix. Substituting $\mathbf{E}^{(0)}$ in Eq.(8) into $\mathbf{E}$ in Eq. (5), the normalized $\mathbf{C}$ at $\mathbf{E}^{(0)}$: $\mathbf{C}^{(1)}$ is:

$$\mathbf{C}'^{(1)} = \frac{\mathbf{S_e}'\mathbf{E}'^{(0)}}{|\mathbf{S_e}'\mathbf{E}'^{(0)}|} \tag{9}$$

The capacitance difference between $\mathbf{C}^{(0)}$ and $\mathbf{C}^{(1)}$: $\Delta\mathbf{C}'^{(1)}$ is:

$$\Delta\mathbf{C}'^{(1)} = \mathbf{C}'^{(0)} - \mathbf{C}'^{(1)} = \mathbf{S_e}'\Delta\mathbf{E}'^{(1)} \tag{10}$$

Therefore, the approximate value of the permittivity difference is :

$$\Delta\mathbf{E}'^{(1)} = \mathbf{S_e}'^{\mathrm{T}}\,\Delta\mathbf{C}'^{(1)} \tag{11}$$

Adding Eq.(8) to the initial permittivity $\mathbf{E}^{(0)}$, the 1st iterative permittivity value $\mathbf{E}$: $\mathbf{E}^{(1)}$ is:

$$\begin{aligned}\mathbf{E}'^{(1)} &= \mathbf{E}'^{(0)} + \Delta\mathbf{E}'^{(1)} = \mathbf{E}'^{(0)} + \mathbf{S_e}'^{\mathrm{T}}\,\Delta\mathbf{C}'^{(1)} \\ &= \mathbf{E}'^{(0)} + \mathbf{S_e}'^{\mathrm{T}} \left(\mathbf{C}'^{(0)} - \frac{\mathbf{S_e}'\mathbf{E}'^{(0)}}{|\mathbf{S_e}'\mathbf{E}'^{(0)}|} \right)\end{aligned} \tag{12}$$

The relation between kth iterative solution $\mathbf{E}^{(k)}$ and $(k-1)$th iterative solution $\mathbf{E}^{(k-1)}$ is:

$$\begin{aligned}\mathbf{E}'^{(k)} &= \mathbf{E}'^{(k-1)} + \mathbf{S_e}'^{\mathrm{T}}\,\Delta\mathbf{C}'^{(k-1)} \\ &= \mathbf{E}'^{(k-1)} + \mathbf{S_e}'^{\mathrm{T}} \left(\mathbf{C}'^{(0)} - \frac{\mathbf{S_e}'\mathbf{E}'^{(k-1)}}{|\mathbf{S_e}'\mathbf{E}'^{(k-1)}|} \right)\end{aligned} \tag{13}$$

Where, $\mathbf{I}_m$ is a $m \times m$ unit matrix, and k is the iterative number.

Evaluation Function

From Eq(7) and Eq.(9), one minus $\mathbf{f}(\mathbf{E}^{(k)})$ is:

$$1 - \mathbf{f}(\mathbf{E}^{(k)}) = 1 - \mathbf{C}'^{(0)} \frac{\mathbf{S_e}'\mathbf{E}'^{(k-1)}}{|\mathbf{S_e}'\mathbf{E}'^{(k-1)}|} \rightarrow 0.0 \tag{14}$$

$\mathbf{C}^{(0)}$ multiplies to the left and right members in Eq(14), Eq(14) becomes:

$$\mathbf{C}'^{(0)} - \mathbf{C}'^{(0)}\,\mathbf{C}'^{(0)} \frac{\mathbf{S_e}'\mathbf{E}'^{(k-1)}}{|\mathbf{S_e}'\mathbf{E}'^{(k-1)}|} \rightarrow \mathbf{O} \tag{15}$$

Where, $\mathbf{O}$ is the zero matrix. Because of $\mathbf{C}^{(0)}\mathbf{C}^{(0)}$ =1.0, Eq.(15) becomes,

$$\mathbf{C}'^{(0)} - \frac{\mathbf{S_e}'\mathbf{E}'^{(k-1)}}{|\mathbf{S_e}'\mathbf{E}'^{(k-1)}|} \rightarrow \mathbf{O} \tag{16}$$

The left member of Eq.(16) is the same as $\Delta\mathbf{C}'^{(k-1)}$ in the iterative solution in Eq.(13). Therefore, the iterative solution in Eq.(13) includes the evaluation function.

Convergence

From Eq.(13), the relation between kth iterative solution $\mathbf{E}^{(k)}$ and $(k-1)$th iterative solution $\mathbf{E}^{(k-1)}$ is:

$$\mathbf{E}'^{(k)} = \mathbf{S}_e'^{T}\mathbf{C}'^{(0)} + \left(\mathbf{I}_m - \frac{\mathbf{S}_e'^{T}\mathbf{S}_e'}{\left|\mathbf{S}_e'\mathbf{E}'^{(k-1)}\right|}\right)\mathbf{E}'^{(k-1)} \tag{17}$$

From Eq.(17), the state transition matrix $\mathbf{T}$ between $\mathbf{E}^{(k)}$ and $\mathbf{E}^{(k-1)}$ is:

$$\mathbf{T} = \mathbf{I}_m - \frac{\mathbf{S}_e'^{T}\mathbf{S}e'}{\left|\mathbf{S}_e\mathbf{E}'^{(k-1)}\right|} = \mathbf{I}_m - \frac{\mathbf{S}_e'^{T}\mathbf{S}_e'}{\left|\mathbf{C}'^{(k-1)}\right|} \tag{18}$$

When assuming that $\mathbf{E}^{(k-1)}$ is equal to the eigen value of the state transition matrix $\mathbf{T}$: λ, because of $\mathbf{T}\mathbf{E}'^{(k-1)} = \lambda\mathbf{E}'^{(k-1)}$,

$$\begin{aligned}\mathbf{E}'^{(k)} &= \lambda\mathbf{E}'^{(k-1)} + \mathbf{E}'^{(0)} = \lambda(\lambda\mathbf{E}'^{(k-2)} + \mathbf{E}'^{(0)}) + \mathbf{E}'^{(0)} \\ &= (\lambda^k + \lambda^{k-1} + \ldots + \mathbf{I}_m)\mathbf{E}'^{(0)}\end{aligned} \tag{19}$$

Because the maximum eigen value of the state transition matrix $\mathbf{T}$: λ_{max} is less than one, Eq.(13) gives the accurate and stable solution in the case of $k \to \infty$.

SIMULATION

LBP, NR and SPM methods are tested using imitation images of particle distribution of solid air two-phase flow. Generally, the iterative solution of NR method is not converged without normalization and gain setting. In this study, the iterative solution of NR method is normalized and set a gain as follows:

$$\begin{aligned}\mathbf{E}^{*(k)} &= \mathbf{E}^{*(k-1)} + \Delta\mathbf{E}^{*(k-1)} \\ &= \mathbf{S}_e^{T}\mathbf{C}^{(0)} + g\left(\mathbf{I}_m - \mathbf{S}_e^{T}\mathbf{S}_e\right)\mathbf{E}^{*(k-1)} \\ \mathbf{E}^{*(k)} &= \frac{\mathbf{E}^{(k)} - \min\mathbf{E}^{(k)}}{\max\mathbf{E}^{(k)} - \min\mathbf{E}^{(k)}} \\ \Delta\mathbf{E}^{*(k)} &= \mathbf{E}^{*(k-1)} - \mathbf{E}^{*(k-1)}\end{aligned} \tag{20}$$

Where, * means normalization, g is a gain value to converge the iterative solution. At every iteration, $\mathbf{E}^{(k)}$ is normalized by the maximum value: $\max\mathbf{E}^{(k)}$, which means the maximum pixel value among whole image of $\mathbf{E}^{(k)}$, and minimum value $\min\mathbf{E}^{(k)}$. NR and SPM methods iterate enough 3,000 times to obtain the final iterative images. The gain g in Eq(20) is fixed to be 0.9. It is confirmed that the error $\Delta\mathbf{E}^{*(k)}$ is converged at the iteration. Fig. 4(1) shows the imitation images with different particle distribution, which are (a) the center of pipeline, (b) the bottom of pipeline and (c) the dispersion in pipeline. The pixel value of the white part indicating particles is 1.0; the pixel value of the black part indicating air is 0.0. The reconstructed images by each method are shown from Figs. 4 (2) to (4). In these figures, the reconstructed images by SPM are much clear; however, the reconstructed images by LBP and NR are blurred. Especially, in the case of the dispersion, SPM method can indicate the four imitated dispersion particles clear; however, LBP and NR cannot indicate the four imitated dispersion particles. For example, in the case of the center particle distribution in Fig.4(1-a), the convergence process of the evaluation function in Eq.(7) is shown in Fig.5. The $\mathbf{f}(\mathbf{E}^{(k)})$ value at the 3,000 iterative times is 0.9972, which is close to 1.0.

Next, in order to estimate each method quantitatively, the image correlation between the original image and the reconstructed images; C_L, is calculated with:

$$C_L = \frac{\sum_{i=1}^{n}\left(\mathbf{E}_L - \overline{\mathbf{E}_L}\right)\left(\mathbf{I}_L - \overline{\mathbf{I}_L}\right)}{\sqrt{\sum_{i=1}^{n}\left(\mathbf{E}_L - \overline{\mathbf{E}_L}\right)^2}\sqrt{\sum\left(\mathbf{I}_L - \overline{\mathbf{I}_L}\right)^2}} \tag{21}$$

Where, $\mathbf{E}_L$ is the reconstructed images as shown from Fig.4-(2) to Fig.4-(4), $\overline{\mathbf{E}_L}$ is the mean pixel value dividing the total value with the total space pixel (=1024), $\mathbf{I}_L$ is the original image as shown in Fig.4-(1), and $\overline{\mathbf{I}_L}$ is the mean pixel value dividing the total value with the total space pixel. Table 1 shows the image correlation between the original image and the reconstructed images. According to the table, in all cases, the image correlation of LBP is the lowest, that of NR is the next, and the correlation of SPM is the highest. For example, in the dispersion case, SPM increases the image correlation by 40.2% to LBP, and SPM increases it by 17.7% to NR.

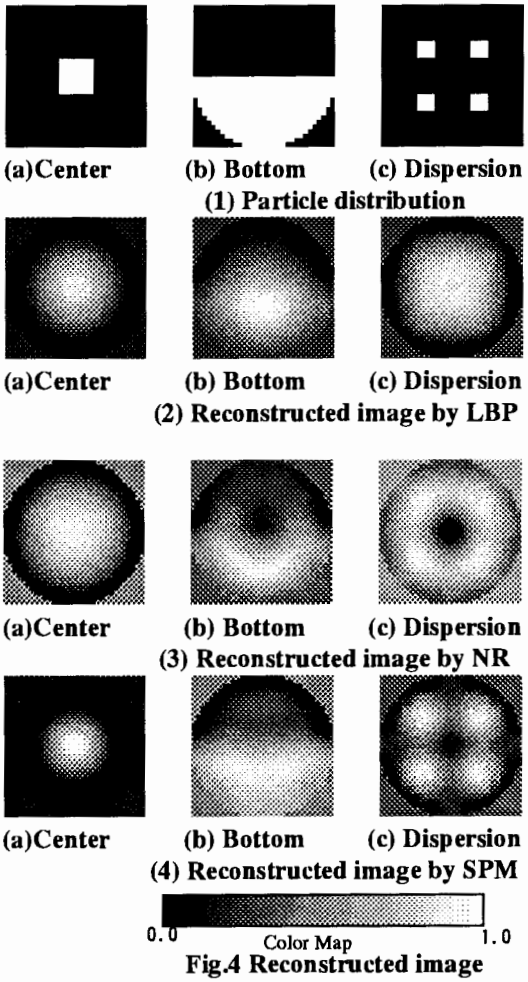

Fig.4 Reconstructed image

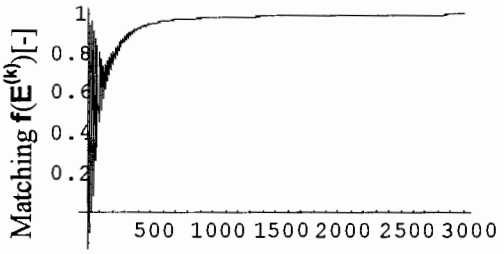

Fig.5 Convergence process of center image by SPM

Table.1 Correlation between original image and reconstructed image

	Center	Bottom	Dispersion
LBP	0.67252	0.641716	0.283811
NR	0.783681	0.474094	0.421036
SPM	0.833886	0.849833	0.598056

EXPERIMENTS

Experimental Equipment, Method & Conditions

In order to compare SPM with NR, real solid air two phase flow images are reconstructed by each method. The experimental equipment is composed of a hopper tank, a vertical pipe, and a receiver tank as shown in Fig.6. The vertical pipe is 49.0 mm inside diameter, and 2.0m long. The CT sensor with 12 electrodes was attached around the circumference at the pipe bottom. The particles, which were almost spherical polyethylene pellets with 3.26mm diameter, 910kg/m^3 density and relative permittivity 2.3, are fallen freely from the hopper tank. The total amount of the particles was 3,000[g] (=5.105 X 10^{-3}[m ^{3}]), and the particle flow rate Qp =6.862 X 10^{-4}[m^3/s]. The time interval to acquire capacitances of 66 pairs of electrodes in a cross section is Δt= 10.0 ms. The measured capacitance at ith pair: $C_m(i)$, normalized with the maximum value 1.0 and minimum value 0.0 by linear calibration as,

$$C^*(i) = \frac{C_m(i) - C_a(i)}{C_p(i) - C_a(i)} \qquad (22)$$

Where, $C^*(i)$ is the normalized capacitance of the ith pair electrodes, $C_p(i)$ is the capacitance at the situation that particles occupy the whole cross-section. $C_a(i)$ is the capacitance at the situation that air occupies the whole cross-section. One image pixel is 1.53×1.53mm^2 because the inside cross-section 49.0 mm is divided with 32×32 image pixels. When a particle core passes through the measurement section, the diameter of one particle holds 2.13 image pixels because the particle diameter is 3.26mm.

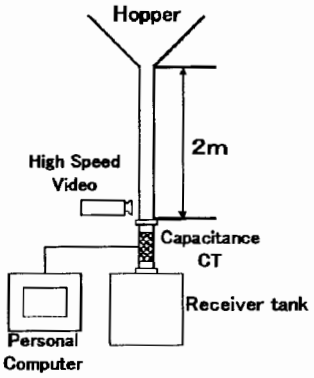

Fig.6 Experimental Equipment

Experimental Results & Reconstructed Images

Fig.7 shows the all normalized capacitances of all electrodes pairs (=66) for 765Δt time (=7.65 second). The x-axis is the time and the electrode pair number, that is, (the quotient of x/66 + 1) × Δt shows the time, and (the modulo of x/66 +1) shows the electrode pair number at the time. The time-step images are reconstructed by NR and SPM methods, based on the normalized capacitances from 200Δt to 550Δt. The reconstruction images by NR method depend on the gain and the iterative number. The iteration to reconstruct images is fixed 30 times in both NR and SPM method. The gain is determined to make the error converged to nearly 0.0 before 30 times iteration using a sample capacitance at 200Δt. Fig.8 (a) shows pixel mean error $\Delta \mathbf{E}^{*(k)}$ in Eq.(20) and $\mathbf{E}^{*(k)}$ images after 30 times iteration in the case of g=0.006, and Fig.8 (b) shows those in the case of g=0.005. The image pixel, where any particles do not exist, is blue. As the particle density in an image pixel becomes high, the image pixel changes into red with 10 stages in the color bar. Because of the image normalization, the reconstruction image does not indicate the real density particle image; but indicates the relative images. From Fig.8, the gain is determined g=0.005 because the pixel mean error $\Delta \mathbf{E}^{*(k)}$ is converged to 0.0 at 30 times iteration. Figs.9 (a) and (b) show the convergence process during the SPM iteration to an image at 202Δt, and the reconstructed image. The final matching value of the evaluation function that is the inner product in Eq.(11) is 0.978, which is nearly 1.0. It means the image is reconstructed, as the capacitance matrix of the reconstructed images: $\mathbf{C}^{(k)}$, matches the experimental capacitance matrix $\mathbf{C}^{(0)}$.

Fig.10(a) shows the representative images reconstructed by NR method at 251, 276, 301, 326, and 351Δt, and Fig.10(b) shows those images by SPM method at the same time. On the whole, the distribution of particle density is qualitatively visualized. The particles density is not uniform because of collisions between particles, particles and pipe wall. Precisely, both images at 251Δt, 301Δt and 351Δt are relatively similar; however, the image patterns at 276Δt and 326Δt are different at the central left part and the around wall, respectively.

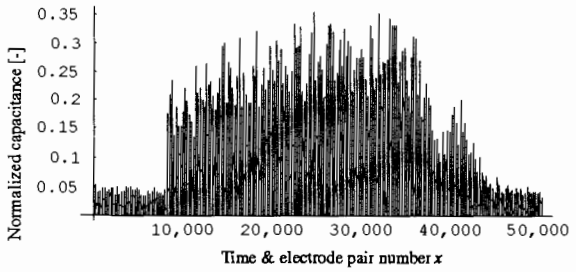

(The quotient of $x/66+1) \times \Delta t$ is time.
(The modulo of $x/66+1$) is electrode pair number at the time.

Fig.7 Capacitances of time and electrode number series

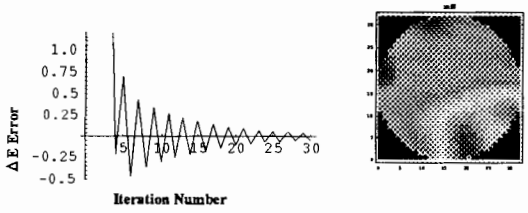

(a-1) Pixel mean error $\Delta E^{*(k)}$ (a-2) Reconstructed image
(a)Gain g=0.006

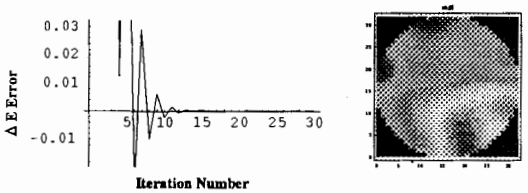

(b-1) Pixel mean error $\Delta E^{*(k)}$ (b-2) Reconstructed image
(b)Gain g=0.005

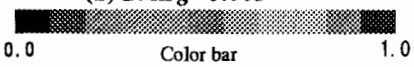

Fig.8 $\Delta E^{(k)}$ error and reconstructed images after iteration

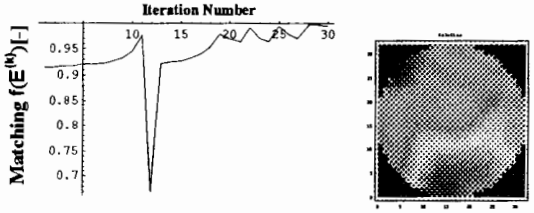

(a) Evaluation function value (b) Reconstructed image

Fig.9 Convergence process during iteration and the image by SPM

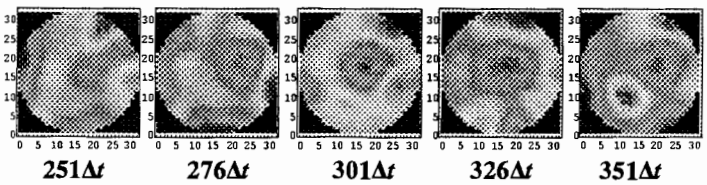

251Δt 276Δt 301Δt 326Δt 351Δt

(a) NR method

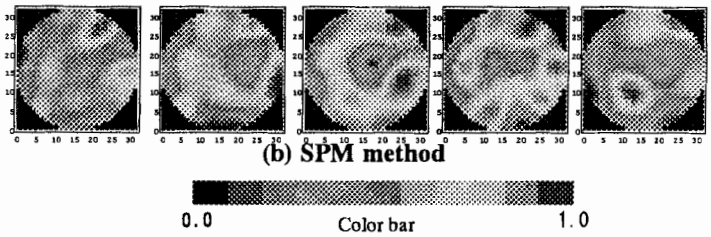

(b) SPM method

Fig.10 Example of reconstructed images

DISCUSSION

Void Ratio Calculation

In order to examine which method between NR and SPM is more accurate, the void ratios are calculated from the images reconstructed by both methods, to compare with the void ratio calculated from the experimental capacitances. The void ratio at time from the experimental capacitances in Fig.7: V_C, is calculated from:

$$V_C = \frac{1}{n}\sum_{i=1}^{n}\left(\frac{C(i)}{C_k}\right)\times 100 \quad [\%] \qquad (23)$$

Where, $C(i)$ is the normalized capacitance value at ith electrodes pear, C_k is a capacitance value of the high dielectric (= 1.0), n is the total electrode pair number (=66). The void ratio becomes 0% when the sensor is satisfied with a low dielectric completely; it becomes 100% when it is satisfied with a high dielectric completely. On the other hand, the void ratio from the picture element pixel in a reconstructed image; V_I, is calculated from:

$$V_I = \frac{k}{m}\sum_{i=1}^{m}\left(\frac{P(i)}{P_k}\right)\times 100 \quad [\%] \qquad (24)$$

Where, $P(i)$ is the normalized dielectric picture pixel value in a cross section, P_k is a high dielectric pixel value (= 1.0), and m is the picture pixel number which is space resolution (=1024). Because the images reconstructed by both methods are normalized at every iteration to result in the relative value, the relative void ratios are compensated with a coefficient k in Eq.(23) to match the time mean void ratio from the experimental capacitances. Which method is more accurate is discussed by the deviation value;

$$f_L = \frac{1}{(ts-te)}\sum_{t=ts}^{t=te}\sqrt{\left(V_{C,t}-V_{I,t}\right)^2} \qquad (25)$$

Where, t_s is the 200, which is the first considered image, and t_e is 550, which is the final considered image. Fig.11 shows the time series of the void ratio calculated from the experimental capacitances. Fig. 12 shows the time series of the void ratio compensated with the coefficient k by NR methods. Fig.13 shows the time series of the void ratio compensated with the coefficient k by SPM method. The table 2 shows the each value. The deviation calculated by SPM: 0.749 is much smaller than that done by NR: 1.73 by 56.7%. It means that

the reconstructed images by SPM indicate the real particle distribution more accurately than those by NR. Above all, SPM method is the more accurate reconstruction technique for solid air two phase flow CT images than NR method.

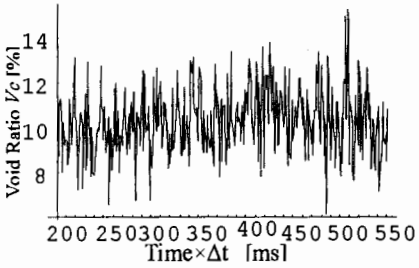

Fig.11 Void ratio from experimental capacitances

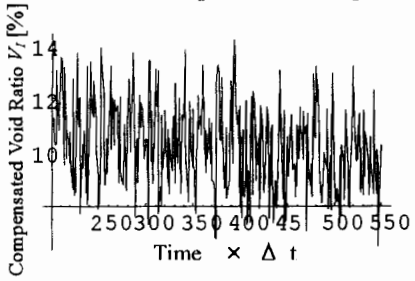

Fig.12 Void ratio from images calculated by NR

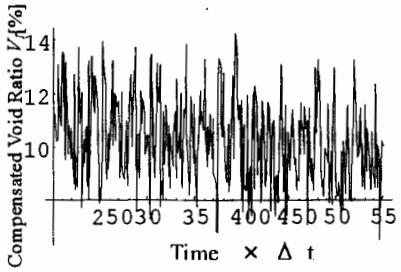

Fig.13 Void ratio from images calculated by SPM

Table 2 Comparison of void ratio by each method

	Coefficient k[-]	Mean void ratio[%]	Max value[%]	Min value[%]	Fluctuation f_L[-]
Capacitance	1.0	10.24	15.28	6.135	-
NR	0.2085	10.24	14.26	6.495	1.73
SPM	292.36	10.24	16.49	3.914	0.749

Correlation to Experimental Capacitances

In order to examine the characteristics of SPM method, the capacitances from the final images by NR and SPM methods are calculated again to obtain the time correlation between the capacitance from the images and the experimental capacitance. Figs.14 (a) – (d) show the experimental capacitance, the capacitance from LBP final image, that from NR final image, and that from SPM final image. Those are normalized between 1.0 and 0.0 to compare easily, and are calculated from the final images at $200\Delta t$ as representative images. Qualitatively, the capacitance from the LBP image does not match the experimental capacitance, the capacitance image from the NR images is getting close to the experimental image, and the capacitance from SPM images match the experimental capacitance. The time series correlation of the capacitance from the images to the experimental capacitance is shown in Fig. 15. The time mean correlation of capacitance from SPM is 0.970; however, those of LBP and NR are very low, which are 0.196 and 0.785. SPM method increases the capacitance matching by 23.6% as compared with NR method because the SPM method has the evaluation function to make the inner product between $\mathbf{C}^{(0)}$ and $\mathbf{C}^{(k)}$ becomes 1.0 in Eq.(7), that is, $\Delta\mathbf{C}^{(k-1)} \rightarrow \mathbf{O}$ in Eq.(13). However, because NR method dose not have any evaluation function, the matching between experimental capacitance and the capacitance from the reconstructed image is not compensated during the irritation process. Especially, in the case that the experimental capacitance shows the high deviation as shown in Fig.14(a), the capacitance by NR method could not trace the pattern of the experimental capacitance without the evaluation function of the inner product. Above all, SPM method is suitable method to reconstruct the solid air two-phase flow CT image.

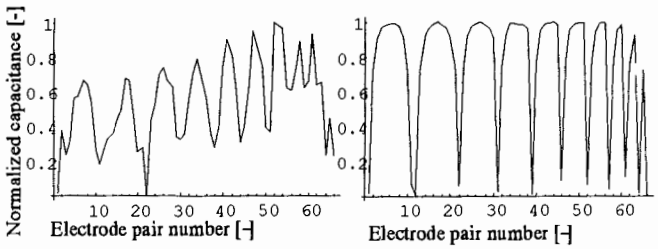

(a) Experimental capacitance **(b) LBP capacitance**

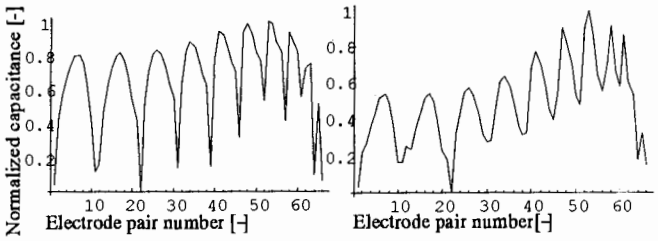

(c) NR capacitance **(d) SPM capacitance**

Fig.14 Capacitances from experiments and reconstructed images

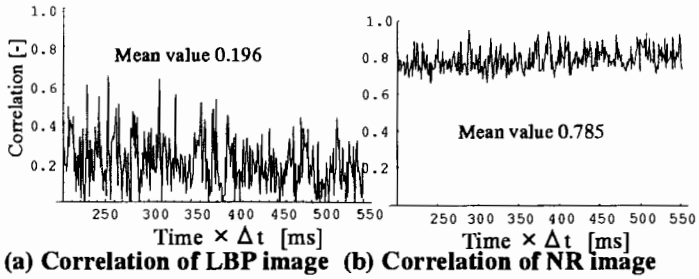

(a) Correlation of LBP image (b) Correlation of NR image

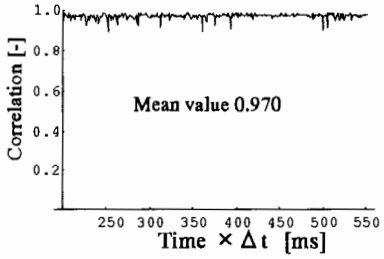

(c) Correlation of SPM image

Fig.15 Correlation between experimental capacitance and that from images

CONCLUSIONS

Sampled pattern mating method (SPM) has been applied to an ill-posed inverse problem of a capacitance-computed tomography for solid air two-phase flow. The results are as follows:

1) The accuracy of the imitated reconstructed image is improved. For example, in the dispersion imitated image case, SPM increases the image correlation by 40.2% to LBP, and SPM increases it by 17.7% to NR.
2) The time-mean deviation of the particles volume ratio between the image and capacitances are calculated. The deviation calculated by SPM: 0.749 is much smaller than that done by NR: 1.73 by 56.7%. It means that the reconstructed images by SPM indicate the real particle distribution more accurately than those by NR.
3) The time mean correlation of capacitance from SPM is 0.970; however, those of LBP and NR are very low. SPM method increases the capacitance matching by 23.6% as compared with NR method because the SPM method has the evaluation function to make the inner product between $\mathbf{C}^{(0)}$ and $\mathbf{C}^{(k)}$ becomes 1.0.

ACKNOWLEDGMENT

The authors greatly wish to thank Dr. Tomsz Dyakowski of UMIST and Mr. Malcolm Byars of PTL in UK for the useful advices.

REFERENCES

Duggan P.M and York T.A, (1995) Tomographic image reconstruction using RAM-based neural networks, *Proc. 4th ECAPT Conf.* (European concerted action on process tomography), Bergen 6-8, April, pp411-419

Dyakowski,T., Luke,S.P., Ostrowski,K.L. and Williams,R.A. (1999) On-line monitoring of dense phase flow using real time dielectric imaging, *Powder Technol*, Vol. 104, 287-295

Huang,S.M., Plaskowski,A.B., Xie,C.G. and Beck,M.S. (1989) Tomographic imaging of two-component flow using capacitance sensors, *J.Phys, E: Sci, Intrrum*, 22 , pp173-177,

Isaksen O and Nordtvedt J.E (1993), A new reconstruction algorithm for process tomography, *Measurement science & technology*, Vol.4, pp1464-1475

Liu.S, Fu.L and Yang.W.Q, (2001) Comparison of three image reconstruction algorithms for electrical capacitance tomography, *Proc. 2nd world congress on industrial process tomography*, Honnover, Germany, pp29-34

Reinecke,N and Mewes,D, (1994) Resolution enhancement for muti-electode capacitance sensor, *Proc. 3rd ECAPT Conf.* (European concerted action on process tomography), Porto, 22-26 March

Xie C.G, Huang S M, Hoyle B.S, Thorn R, Lenne C and Beck. M.S, (1992), Electrical capacitance tomography for flow imaging, *IEE Proc.* G 139 pp89-98